Early-stage flame acceleration in stratified hydrogen-air mixtures: Theory and simulation

Sébastien Missey, Omar Dounia, Laurent Selle

Proceedings of the Combustion Institute 40 (2024) 105279

Contents lists available at ScienceDirect

Proceedings of the Combustion Institute

journal homepage: www.elsevier.com/locate/proci

Early-stage flame acceleration in stratified hydrogen-air mixtures: Theory and simulation

Sébastien Missey [a,*], Omar Dounia [b], Laurent Selle [a]

[a] Institut de Mécanique des Fluides de Toulouse, IMFT, Université de Toulouse, CNRS, Toulouse 31400, France
[b] CERFACS, 42 Avenue Gaspard Coriolis, Toulouse Cedex 01 31057, France

ARTICLE INFO

Keywords:
Hydrogen
Direct Numerical Simulation
Finger flame theory
Stratified composition
Stratified temperature

ABSTRACT

The use of hydrogen as an energy vector calls for an in-depth analysis of the associated risks and the development of mitigation strategies. In the case of liquid hydrogen storage, there are virtually no norms for uses concerning the general public and there is little background on safety measures for an industrial use –with the notable exception of rocket propulsion, which is a very specific domain. The present works addresses the accidental release of liquid hydrogen, resulting in a pool that would create a flammable cloud because of its fast evaporation. This cloud is characterized by strong temperature and composition gradients that are likely to strongly affect the propagation of a flame kernel, in the event of an accidental ignition. The present work is dedicated to the prediction of the initial acceleration of the flame front in a canonical case: a tube with an axial stratification typical of a liquid-hydrogen spill. Numerical simulations and analytical developments are performed and compared in order to unravel the driving mechanisms and identify the risks of various scenarios. It is shown that ignitions in lean regions may be particularly hazardous because of flame-front instabilities as well as composition gradients favoring acceleration.

1. Introduction

Hydrogen is a promising energy vector for the decarbonization of many sectors, including industry, transportation and heating. One of the major issues with hydrogen is its low power density per volume. As a solution, two technologies are employed: compression up to 700 bar and liquefaction. The use of liquid hydrogen will require new safety regulations and procedures that are yet to be defined. An accidental release will create a hazardous environment, where an ignition may have disastrous consequences. Some studies have already been performed in order to assess the risks associated with an hydrogen spill on the ground. In the late 50's, Little [1] reported on a series of experiments where various amounts of liquid hydrogen were spilled and ignited. One of the main findings was that no transition to detonation was observed in this series. An other large liquid hydrogen spill was performed by Witcofski et al. [2], to analyze the cloud resulting from a release and one of the conclusions was that the flammable region resulting from a rapid spill would dissipate faster than that of a slow spill. More recently, a large number of experiments and simulation with cryogenic hydrogen were performed during the PRESLHY Project [3]. In the so-called pool experiment [4], where liquid hydrogen is spilled over different soils (concrete, sand, gravel, etc.) placed in a bucket and subsequently ignited, huge damage was recorded in one case and attributed to a liquid hydrogen-condensed oxygen explosion.

A liquid-hydrogen spill on the ground is a strongly multiphysics phenomena. Heat transfer from the ground drives the evaporation rate of the pool. Mixing is controlled by a combination of buoyancy and/or convective effects. Additionally, because of the extremely low temperature of liquid H_2 (< 20 K), water vapor usually freezes and nitrogen and oxygen can also liquefy and even freeze as well. The result is a strongly stratified plume with temperature and hydrogen concentration gradients, as well as potential liquid or solid particles. This is likely to strongly affect flame propagation. First, Cheikhravat et al. [5] have shown that the impact of water on flame propagation depends on the droplet sizes' distribution. The influence of variable hydrogen content on flame propagation was also the subject of many studies, mainly in closed tubes/channels. For example the so-called Gravent database from TUM [6] is a reference for H_2/Air with stratification and water mist. One of the main conclusions of this study is that a transverse gradient yields a stronger flame acceleration and shorter distance for the transition to detonation. Finally, several studies were also dedicated to the effect of cryogenic temperature on flame propagation. Kuznetsov et al. [7] showed that, compared to ambient conditions, H_2-air mixtures at temperatures close to cryogenic exhibit

* Corresponding author.
E-mail address: sebastien.missey@imft.fr (S. Missey).

https://doi.org/10.1016/j.proci.2024.105279
Received 4 December 2023; Accepted 22 May 2024
Available online 1 July 2024

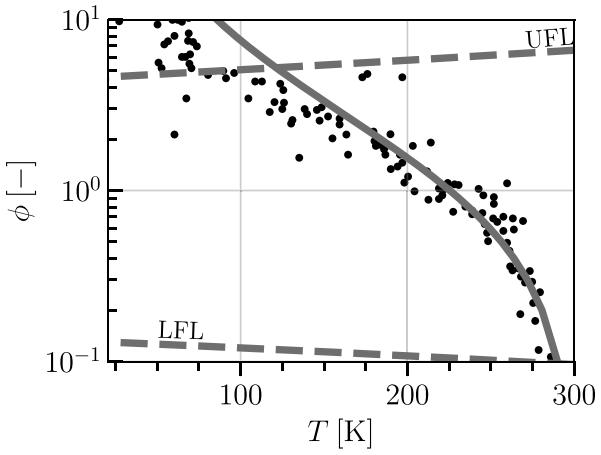

Fig. 1. Relation between equivalence ratio ϕ and temperature T in the cloud above a liquid hydrogen spill: (•) PRESLHY experiment [10]; (—) perfect mixing $\phi = p_m(T)$. Upper (UFL) and Lower (LFL) flammability limits are also shown.

a stronger flame acceleration, reduced run-up distances to detonation (by half) and higher detonation pressures (2 to 3 times). Recent work by Shen et al. [8] confirm these findings for hydrogen–oxygen mixtures at even lower temperature and initial pressure.

On the numerical side, the flame acceleration enhancement by low-temperature mixtures was successfully reproduced by Yang et al. [9]. Unfortunately, to the authors' knowledge, the case of simultaneous gradients in temperature and hydrogen content has not been addressed, despite its crucial importance in scenarios encountered in an accidental spill of liquid hydrogen. Indeed, Fig. 1 shows the relation between the local equivalence ratio ϕ and the temperature T in the plume of an evaporating pool of liquid hydrogen. A perfect mixing relation, describing the ideal mixing between cold H_2 and ambient air, is shown to match fairly closely the experimental results of the PRESLHY project [10], especially at relatively high temperatures $T \geq 150$ K. The gap observed at lower temperatures can be attributed to the presence of condensed water in the experiment, not taken into account in the perfect mixing relation. The upper and lower flammability limits [11], indicate the conditions where the mixture above the pool can ignite and produce a flame kernel. The paper will therefore focus on the region between these two limits and will consider stratification cases consistent with the conditions found above a liquid H_2 pool (mixing relation $\phi = p_m(T)$ will be used to link temperature and composition).

The objective of the present work is to evaluate the influence of the stratification on the propagation of a flame front above a liquid H_2 pool. As a first step, this problem is addressed in the canonical configuration of ignition in a tube, which allows to study the combined effect of wall-confinement and stratification on flame acceleration. In Section 2 numerical simulations, based on the framework developed in [12] are conducted. Then, the theory governing the early stages of flame acceleration in tubes, based on the work of [13], is extended to account for mixture stratification in Section 3 and confronted to the simulations in Section 4.

2. Numerical investigation of flame acceleration under mixture stratification

This part of the paper investigates numerically the early stages of flame acceleration in mixtures with axially stratified temperature and mixture composition.

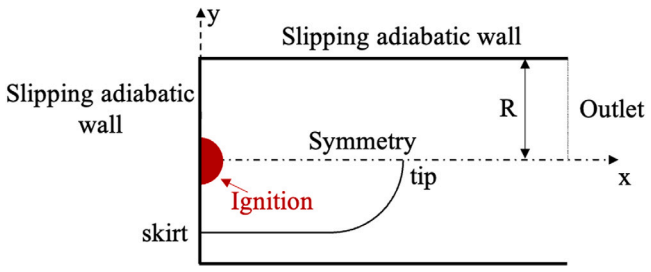

Fig. 2. Configuration used for the study of the early stages of flame acceleration: boundary conditions of the simulation on the top half tube and flame characteristic shape on the bottom half tube.

Table 1
Initials conditions of simulation with stratification. $\Delta T_{x=R} = \pm 24$ K, depending of the initial gradient.

Case	At $x = 0$	∇T [K/m]	$\Delta\phi_{x=R}$
A	$T_0 = 225.4$ K $\phi_0 = 1.0$	0	0
A-1		−1200	0.514
A-2		1200	−0.397
B	$T_0 = 138.0$ K $\phi_0 = 4.0$	1200	−1.216
C	$T_0 = 263.9$ K $\phi_0 = 0.4$	−1200	0.352

2.1. Numerical setup

The numerical investigation is performed using the massively parallel solver AVBP [14], developed by CERFACS. It solves the multispecies, compressible reactive Navier–Stokes equations on unstructured meshes. It is a cell-vertex/finite element code, explicit in time. The configuration of interest is two-dimensional and sketched in Fig. 2. A tube of radius $R = 20$ mm and length $L = 5R$, closed on one end and open on the other is considered. Only half of the tube will be simulated and a symmetry condition is imposed on the central axis. An adiabatic and slip wall condition is imposed on the closed end and top boundary conditions. A non-reflecting boundary condition is used for the open end of the tube with a NSCBC formalism [15]. A small kernel (radius 1 mm) of hot combustion products is used to ignite the mixtures at the closed end of the tube. A constant pressure, $P = 1$ atm, and quiescent mixture is set initially inside the tube. Both homogeneous and axially-stratified temperature fields are imposed initially and the perfect-mixing relation in Fig. 1 is used to set the mixture composition from temperature field, thereby mimicking the conditions encountered above a liquid H_2 pool. The flame properties at the location of ignition ($x = 0$) are denoted by the subscript $*_0$ and used as scaling parameters in the paper.

Table 1 recalls the conditions considered in the present work and Fig. 3 displays the evolution of associated flame properties (their spatial profile is also provided in the supplementary material for completeness). Both the planar consumption speed s_L and the gas expansion ratio $\sigma \equiv \rho_u/\rho_b$ are shown, where ρ_u and ρ_b are the unburnt and burnt gas densities, respectively. For cases A, A-1 and A-2, the condition at the ignition point is set to $T_0 = 225.4$ K corresponding to a stoichiometric mixture. The mixture is homogeneous in case A and a negative (resp. positive) constant temperature gradient is imposed for cases A-1 (resp. A-2). Cases A-* correspond to a flame ignited at the stoichiometric condition and propagating either towards (A-1) or away from (A-2) the liquid pool. As shown in Fig. 3, the mixture stratification in cases A-* is imposed such that the flame will propagate towards more (A-1) or less (A-2) reactive mixtures with initially increasing (resp. decreasing) s_L and σ.

Case B corresponds to the scenario where the flame is ignited at rich conditions close to the liquid pool and essentially propagates

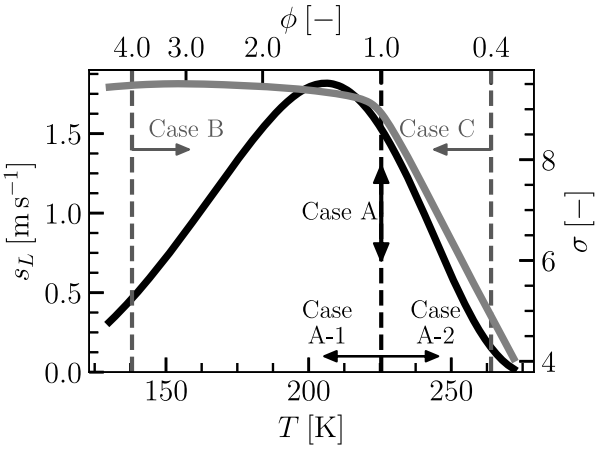

Fig. 3. Evolution of the planar consumption speed s_L ( ) and expansion factor $\sigma \equiv \rho_u/\rho_b$ ( ) with mixture conditions. Temperature and equivalence ratio are linked by the perfect mixing relation. Arrows indicate the direction of the temperature-composition stratification.

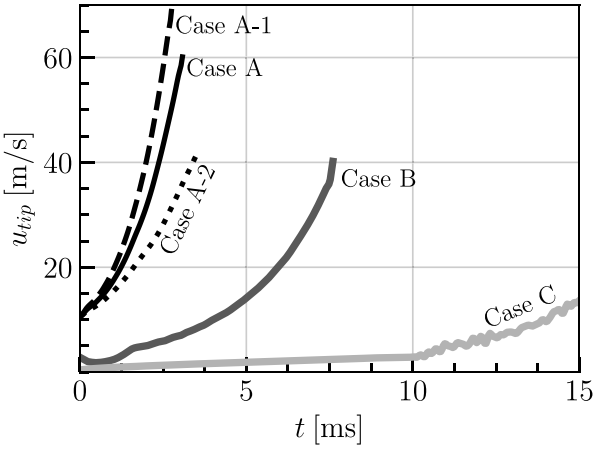

Fig. 4. Evolution of the flame propagation speed u_{tip} versus time t for Case A ( ), Case A-1 ( ), Case A-2 ( ), Case B ( ) and Case C ( ).

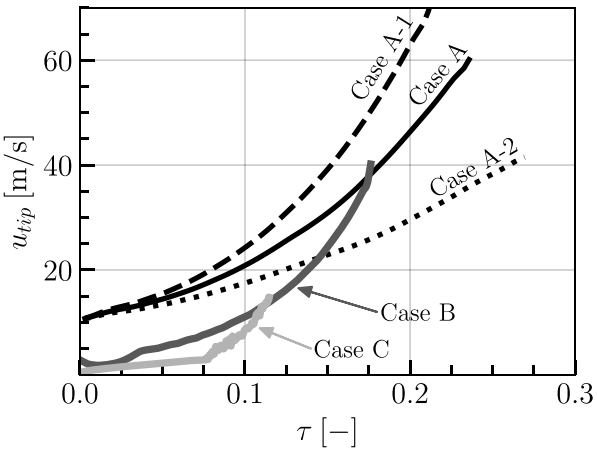

Fig. 5. Evolution of the flame propagation speed u_{tip} versus normalized time $\tau \equiv s_{L,0}t/R$ for Case A ( ), Case A-1 ( ), Case A-2 ( ), Case B ( ) and Case C ( ).

away from the pool, hence the positive temperature gradient. Finally, case C corresponds to the scenario where the flame is ignited at very lean conditions far away form the pool and propagates towards more reactive mixture conditions that can be found closer to the liquid pool, hence the negative temperature gradient. Note that in both cases B and C, the flame propagates towards more reactive mixtures as highlighted in Fig. 3. The magnitude of ∇T is the same for both cases.

The same mesh is used for all the simulations. The cell size (δ_{cell} = 31.6 μm) is uniform inside the tube and ensures at least 8 cells within the front with the smallest laminar thermal flame thickness δ_T^0 among the conditions considered in Table 1, i.e. at T = 191 K and ϕ = 1.8. The San Diego [16] chemical scheme is used to model H_2/air kinetics, without the NOX sub-model. The validity of the San-Diego mechanism up to temperature conditions relevant for the present work is verified in the supplementary material. A simplified transport model for the species is used with constant mixture Prandlt number and a constant Schmidt number for each species. The second-order in space and time Lax–Wendroff scheme is used for the advection term and a second-order finite-volume scheme is used for the diffusion terms. The perfect gas equation of state is used. The validity of this assumption for the initial conditions considered in this work is verified in the supplementary material.

2.2. Numerical results and discussion

This section is devoted to the analysis of flame acceleration observed in the simulations. The flame-tip position x_{tip} is tracked over time. As highlighted in Fig. 2, x_{tip} is defined as the axial position of the flame front on the symmetry axis, which coincides exactly with the axial position of the flame leading point x_{max} for cases A–B, in accordance with the finger flame theory [13] and is close to x_{max} for case C, as discussed later. The flame propagation speed is simply defined by $u_{tip} = \partial_t(x_{tip})$.

Fig. 4 displays the evolution of u_{tip} versus the time t for all cases. The initial flame speed is identical for cases A, A-1 and A-2 since they share the same initial conditions at the ignition point. Because of the confinement induced by the side wall, the homogeneous case A exhibits an exponential-like evolution of the flame speed with time, as predicted theoretically [13].

The impact of mixture stratification can be assessed by comparing case A, with A-1 and A-2. While case A-1 clearly enhances flame acceleration, the opposite effect is observed with case A-2. This result can be attributed to the gradient of flame properties associated to the stratification imposed initially. As shown in Fig. 3, the flame in case A-2 propagates towards a less reactive mixture with decreasing planar consumption speed s_L and gas expansion factor σ, thereby explaining the mitigation effect that stratification has on flame acceleration on this case. For cases B and C, the flame propagation speed u_{tip} (Fig. 4) is initially much lower than cases A* owing to the smaller spherical flame expansion velocities $\sigma_0 s_{L,0}$ at the ignition conditions: $\sigma_0 s_{L,0}$ = 13.6($A*$), 4.39(B) and 0.73(C). Overall, cases B and C also show an exponential-like flame speed evolution with time, albeit much lower flame speeds compared to cases A* (especially case C), due to the lowest reactivity of the mixtures involved (more specifically, lower initial $\sigma_0 s_{L,0}$).

The results of Fig. 4 are displayed in Fig. 5 using a time $\tau \equiv s_{L,0}t/R$ normalized by the initial laminar flame speed $s_{L,0}$ and the tube radius R. In this new coordinate system, the slope of the $u_{tip} - \tau$ curves is much more pronounced for cases B and C compared to cases A*, thereby suggesting that cases B and C undergo a much stronger flame acceleration than cases A* relative to their initial reactivity.

An indication of the mechanisms driving the flame accelerations observed in the simulations is found in Fig. 6, which shows the flame shape for all cases at the same normalized time τ = 0.1 (the evolution in time of the flame shape is also provided in the supplementary material). The homogeneous case A exhibits a finger-like shape, further confirming that the flame acceleration in case A is induced by the strong

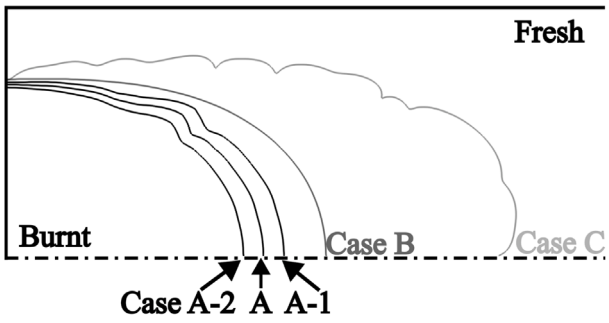

Fig. 6. Flame surface at an isoline of temperature $T = 350$ K, for the different Case at $\tau = s_{L,0}t/R = 0.1$.

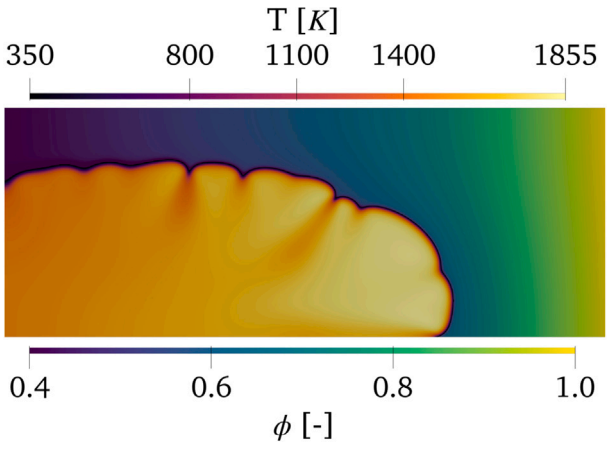

Fig. 7. Simulation Case C at $\tau = 0.1$, with temperature in burnt gases and equivalence ratio in fresh gas.

confinement caused by the presence of the side wall in accordance with the finger flame theory. The stratified cases A-1, A-2 and B exhibit the same finger-like shape, thereby suggesting that wall confinement also drives the flame acceleration observed in Fig. 5 in stratified cases and that stratification plays an enhancing role in cases A-1 and B (hence a stronger flame acceleration) and a mitigating role for case A-2 (reduced flame acceleration compared to A). Case C stands out from all other cases and exhibits an overall finger-flame shape with a marked cellular structure. This is caused by thermo-diffusive instabilities characteristic of very lean H_2/air flames, which enhance the finger flame acceleration as highlighted in [12].

Further emphasis is put on case C in Fig. 7, where the temperature field in the burnt gases and the field of equivalence ratio in the unburnt mixture ahead of the flame are displayed. The image is truncated to focus on the fame region. At $\tau = 0.1$, the flame front is fed by hydrogen/air mixtures over a wide range of equivalence ratios ranging from $\phi \approx 0.8$ at the flame tip to $\phi \approx 0.4$ close to the ignition plate. This has a direct impact on the temperature field in the burnt gases with higher temperatures close to the flame tip. Therefore, Fig. 7 suggests that the flame acceleration observed for case C is the result of a synergistic coupling between wall confinement, mixture stratification and thermo-diffusive instabilities. Temperature and equivalence ratio fields for all the cases are provided in the supplementary material.

The present simulations suggest a potential enhancement of the explosion hazards in case of ignition above H_2 liquid pools. A coupling between wall-confinement and mixture stratification effects is highlighted. The next section delves into the theoretical modeling of this phenomenon by revisiting the finger-flame theory to include the effects of stratification.

3. Extension of finger flame theory to mixture stratification above hydrogen liquid pools

The early stages of flame acceleration in a tube are fairly well described by the finger flame theory proposed in [13] for the case of an homogeneous mixture. The theory was also extended to account for compressibility effects in [17], which become important for highly reactive mixtures like H_2/O_2 near stoichiometry. In the present work, it is extended to cases with axial stratification in a manner analogous to [18] who addressed the case of radial stratification. A derivation is sought, accounting for the combined effects of temperature and composition stratification associated to mixtures above a liquid-hydrogen pool (Fig. 1). This will serve as the baseline tool to analyze the results of Section 2.

The derivation follows the one proposed in [13] and will be briefly exposed in this section, with particular emphasis on the modifications needed to account for mixture stratification. Similarly to the configuration studied in Section 2, a 2D cylindrical tube of radius R with one end closed is considered here. The flame is ignited at the end wall at the symmetry axis. The initial mixture stratification is represented by an axial gradient of temperature and equivalence ratio ($\partial_x(T) \neq 0$, $\phi = p_m(T)$). The tube radius R and the planar consumption speed $s_{L,0}$ taken at the ignition wall is used for scaling: $\tau \equiv s_{L,0}t/R$, $(\xi, \eta) \equiv (x, y)/R$ and $(v, w) \equiv (u_x, u_y)/s_{L,0}$.

The finger flame theory focuses on the evolution of two particular points on the flame front, indicated in Fig. 2: the flame position at the ignition wall (flame skirt) and the flame position on the symmetry axis (flame tip). The whole derivation essentially relies an four hypotheses: ($\mathcal{H}1$) infinitely thin flame front; ($\mathcal{H}2$) irrotational flow at the vicinity of the ignition wall ($\xi \to 0$) and to the symmetry axis $\eta \to 0$ and ($\mathcal{H}3$) locally planar flame front close to the two points of interest (tip and skirt). Hypotheses ($\mathcal{H}2$-$\mathcal{H}3$) are mutually consistent.

For simplicity, the flow is considered incompressible here (see [17] for compressibility effects) and the flow is described by the continuity equation:

$$\frac{\partial \rho v}{\partial \xi} + \frac{\partial \rho w}{\partial \eta} = 0 \tag{1}$$

We are interested in the flow in the burnt and unburnt regions, separated by the flame front and denoted by $*_b$ and $*_u$ respectively. Solutions to Eq. (1) close to the wall ($\xi \to 0$) are obtained under a potential flow assumption, following ($\mathcal{H}2$), for the axial velocity under the boundary condition $v = 0$ at $\xi = 0$:

$$\rho_u v_u = \rho_{u,0} A_u \xi, \quad \rho_b v_b = \rho_{b,0} A_b \xi \tag{2}$$

A_u and A_b can be time-dependant and the impact of axial stratification is through variable densities $\rho_b \neq \rho_{b,0}$ and $\rho_u \neq \rho_{u,0}$ for $\xi > 0$. Focusing on the region close to the ignition wall ($\xi \to 0$), solutions to Eqs. (1)–(2) read:

$$\text{Unburnt flow:} \quad v_u = A_u \xi, \; w_u = A_u(1 - \eta) \tag{3}$$

$$\text{Burnt flow:} \quad v_b = A_b \xi, \; w_b = -A_b \eta \tag{4}$$

where the boundary conditions $w_u(\eta = 1) = 0$ and $w_b(\eta = 0) = 0$ have been taken into account. The system of flow Eqs. (3)–(4) is closed by including the jump conditions across the flame front $\eta = \eta_f$:

$$w_u - w_b = \sigma_0 - 1; \quad v_u - v_b = 0 \tag{5}$$

$$\frac{\partial \eta_f}{\partial \tau} - w_u(\eta_f) = 1 \tag{6}$$

where Eq. (5) describes the jump in normal component and continuity of the tangential component of velocity across the flame front. Eq. (6) expresses a fixed flame propagation velocity $s_{L,0}$ with respect to fresh gases. These jump relations allow to fix the velocity parameters $A_u = A_b = \sigma_0 - 1$ and lead to the following equation governing the evolution of the radial position of the flame skirt:

$$\frac{\partial \eta_f}{\partial \tau} - (\sigma_0 - 1)(1 - \eta_f) = 1 \tag{7}$$

This equation for the flame skirt is exactly the same as the homogeneous case, owing to the fact that mixture composition is constant across the ignition plate in the case of axial stratification.

Focusing on the flame tip, an equation governing the evolution of its axial position can also be found. Following ($\mathcal{H}3$), the flame tip propagates at the planar speed σs_L with respect to burnt gases, hence:

$$\frac{\partial \xi_{tip}}{\partial \tau} - v_b(\xi_{tip}) = (\sigma s_L)(\xi_{tip}) \tag{8}$$

where σs_L varies with the flame position because of the axial stratification. The axial velocity v_b on the symmetry axis obeys the potential flow relation (2) and must coincide with Eq. (4) as $\xi \to 0$, hence :

$$v_b = \frac{\rho_{b,0}}{\rho_b}(\sigma_0 - 1)\xi \tag{9}$$

Eq. (8) now reads:

$$\frac{\partial \xi_{tip}}{\partial \tau} - (\sigma_0 - 1) f_{\rho_b}(\xi_{tip})\xi_{tip} = \sigma_0 f_{\sigma s_L}(\xi_{tip}) \tag{10}$$

$$\text{with:} \quad f_{\rho_b} \equiv \frac{\rho_{b,0}}{\rho_b}, \text{ and } \quad f_{\sigma s_L} \equiv \frac{\sigma s_L}{\sigma_0 s_{L,0}} \tag{11}$$

This equation governs the evolution of the flame propagation speed $\partial \xi_{tip}/\partial \tau$. The difference between Eq. (10) and the one obtained in [17] for the homogeneous case lies in the presence of two stratification terms f_{ρ_b} and $f_{\sigma s_L}$, which account for the impact of stratification on burnt gas density (thermal expansion) and flame properties respectively. They reduce to unity in the homogeneous case. Eq. (10) involves ξ_{tip}-dependant parameters $f_i(\xi_{tip})$ and cannot be solved analytically in the general case. It will be solved numerically in the present work. We stress that solving Eq. (10) requires a knowledge about the unburnt-gases properties at the flame tip position $f_i(\xi_{tip})$. A simple closure is to assume a frozen stratification, where the mixture composition and temperature are not impacted by flame propagation and are equal to their value imposed before ignition. Because the fresh gases are set in motion by combustion, this is a crude assumption and Eq. (10) may require a closure model for the evolution of the effective stratification:

$$\text{Frozen stratification:} \quad f_i(\xi) = f_i(\xi)\big|_{\tau=0} \tag{12}$$

$$\text{Effective stratification:} \quad f_i(\xi) = f_i(\xi, \tau) \tag{13}$$

The implications of the frozen stratification assumption (12) and the ability of Eq. (10) to explain the numerical results of Section 2 will be addressed in the next section.

4. Mechanisms of finger flame acceleration under stratification

4.1. Flame skirt behavior: cases A*

First, the theoretical description of the flow close to the ignition wall is confronted to the numerical results of Section 2. Fig. 8 displays the evolution of the flame skirt speed $\dot{\eta}_f$ with its radial position η_f for the simulations A* and the theoretical solution Eq. (7). First, the numerical results clearly show that axial stratification has no impact on the behavior of the flame skirt close to the wall, in accordance with the theory. Second, the deceleration of the flame skirt as it approaches the side wall is also accurately predicted by the theory (slope of the curve $\dot{\eta}_f = f(\eta_f)$ given by the thermal expansion term $\sigma_0 - 1$ in Eq. (7)). Note that, contrary to the theoretical prediction Eq. (7), the flame skirt in the numerical simulations propagates with non-zero radial velocity towards the side wall until it reaches the extreme vicinity of the wall, a consequence of the corner-type flow governing this region and not taken into account in the theory. Nevertheless, despite the simplicity of the derivation proposed in Section 3, it provides an accurate description of the flame skirt behavior close to the ignition wall.

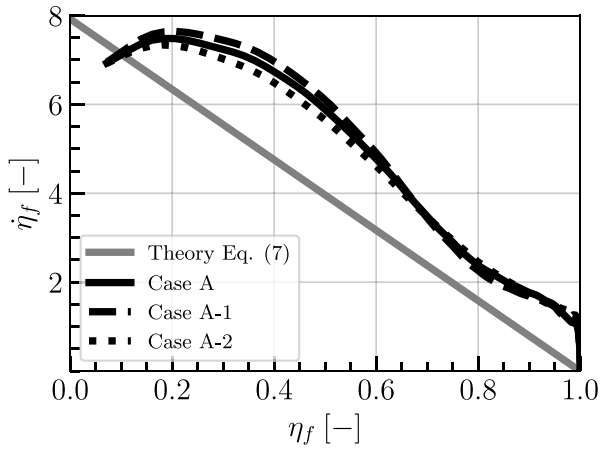

Fig. 8. Evolution of the flame skirt speed $\dot{\eta}_f \equiv \partial \eta_f / \partial \tau$ with its radial position η_f extracted from the numerical simulations for Case A (▬), Case A-1 (▪ ▪) and Case A-2 (▪▪▪). The theoretical solution of Eq. (7) is shown in (▬).

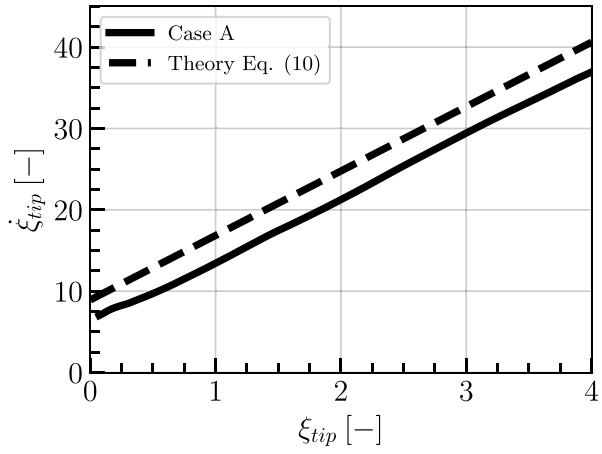

Fig. 9. Evolution of the flame propagation speed $\dot{\xi}_{tip}$ with the flame position ξ_{tip}. Simulation results of Case A (▬) compared to the theoretical prediction of Eq. (10) (▪ ▪), with $f_{\rho_b} = f_{\sigma s_L} = 1$.

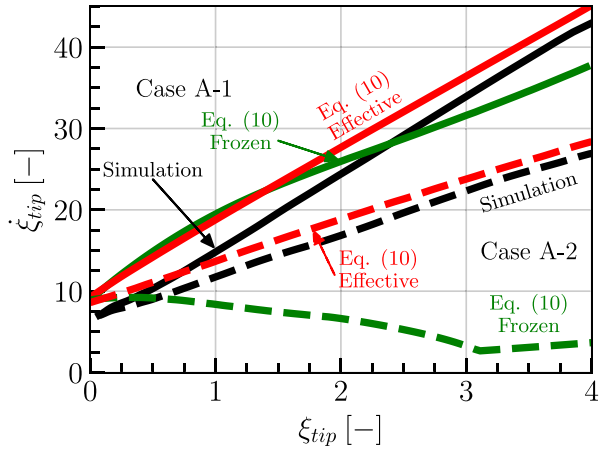

Fig. 10. Evolution of the flame propagation speed $\dot{\xi}_{tip}$ with the flame position ξ_{tip}. Simulation results of Case A-1 (▬) and Case A-2 (▪ ▪) are compared to the theoretical prediction of Eq. (10) under frozen stratification closure (12) (green) and imposing the effective stratification (13) from the simulation (red).

4.2. Flame tip behavior: cases A*

The focus is now on the evolution of the flame tip position. Figs. 9 and 10 compare the evolution of the flame tip velocity $\dot{\xi}_{tip} \equiv \partial\xi_{tip}/\partial\tau$ versus flame-tip position ξ_{tip} obtained numerically (cases A*) to the theoretical value given by Eq. (10). As already demonstrated in [17], Fig. 9 shows that the homogeneous finger-flame theory ($f_{\rho_b} = f_{\sigma s_L} = 1$) is fairly accurate for case A. The extension to stratified cases (Eq. (10)), given by Fig. 10, under the frozen stratification assumption (12) performs reasonably well for the stratified case A-1. For case A-2, however, the theory predicts that the stratification (here towards less reactive mixtures) dominates the finger flame mechanism and induces a deceleration of the flame, which is not observed in the simulation. The reason behind this contrasted performance can be found in Fig. 11, where the initial stratification is compared with the effective stratification that the flame actually feels as it propagates through the mixture. The latter is computed by extracting the mixture conditions, a distance of $3\delta_{L,0}$ ahead of the flame tip, and deducing the effective flame acceleration parameters $f_{i,effective}$ in Eq. (10) during the whole propagation phase. Fig. 11 shows that the effective mixtures burnt by the flame are much closer to the conditions seen initially by the flame close to the ignition plate, owing to the fact that the flame acts as a permeable piston pushing the gas ahead of it, thereby "smoothing out" the axial stratification imposed before ignition. Moreover, Fig. 11 also shows that cases with stronger initial stratification (case A-2) exhibit a larger gap between the effective and frozen stratification parameters with relative gaps $(f_{i,frozen} - f_{i,effective})/f_{i,frozen}$ at $\xi_{tip} = 2$ of approximately 250% and 30% for cases A-2 and A-1, respectively. This implies that the flame propagation has a mitigating effect on the actual conditions at the flame front, owing to the piston effect induced on the flow ahead of it, and that this mitigating effect increases with stronger initial stratification. This explains the contrasted performance of Eq. (10) under frozen stratification closure (see Fig. 10) which accuracy decreases with stronger initial stratification.

Fig. 11 suggests that the frozen stratification assumption, also adopted in [18], is not valid especially for strong stratification cases and Eq. (10) requires an additional evolution equation for the stratification. This is beyond the scope of the present study and will be addressed in a future work. An a posteriori test is performed however where the effective flame acceleration parameters extracted from the simulations are used to close Eq. (10). The results are shown in Fig. 10 where a drastic improvement of the theoretical predictions is observed leading to the conclusion that the extension of the finger flame theory to axial mixture stratification does provide a reliable description of the flame acceleration mechanism at play, which remains essentially a wall confinement effect (finger flame) either enhanced ($f_i > 1$, A-1) or mitigated ($f_i < 1$, A-2) by the mixture stratification. The deviation from the homogeneous case is entirely controlled by the gradient of reactivity imposed by the effective stratification, *i.e.* by how much f_i deviates from unity.

4.3. Flame tip behavior: cases B and C

Fig. 12 confronts the evolution of the flame tip speed obtained with the numerical simulations with the predictions of Eq. (10). The same conclusions drawn for cases A* are still valid for case B and the theoretical curves provide a reasonable agreement with the simulations, especially when the effective flame acceleration parameters, measured in the simulation, are imposed, showing that the present theory is able to take into account changes in the mixture conditions, i.e. ignition location in the cloud above a hydrogen liquid spill. The evolution of the effective stratification parameters $f_{i,effective}$ for cases B and C is not shown here for conciseness but is provided in the supplementary materials. Case C stands out again from the other cases. Imposing the effective parameters mitigates the strong flame acceleration observed with the frozen stratification assumption as expected but is still far from the simulation result. The remaining gap between the effective theory and the simulation is attributed to the intrinsic thermo-diffusive instability characteristic of very lean hydrogen/air mixtures as already highlighted in Figs. 6–7. This result is consistent with the findings of [12] who demonstrated the instability-induced enhancement of the finger flame acceleration. Of course, the finger flame theory does not account for any flame-front stretch effect and predicting the flame acceleration for very lean hydrogen-air mixtures with high accuracy is a limitation of the current theory.

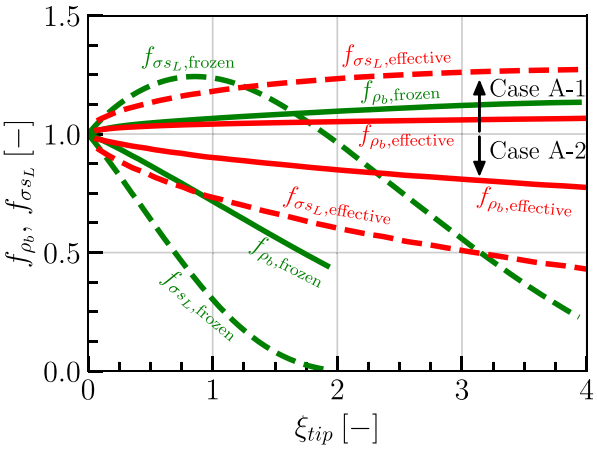

Fig. 11. Evolution of the flame acceleration parameters f_{ρ_b} and $f_{\sigma s_L}$ in Eq. (10) with the flame position. Frozen conditions (12) (green) are compared to the effective conditions (13) extracted from the simulations (red). Case A-1 and A-2 are shown in the upper and lower parts respectively.

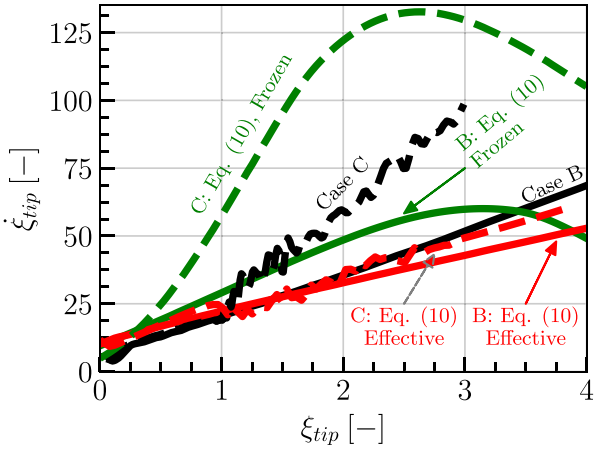

Fig. 12. Evolution of the flame propagation speed $\dot{\xi}_{tip}$ with the flame position ξ_{tip}. Simulation results of Case B (▬) and C (▪ ▪) are compared to the theoretical prediction of Eq. (10) under frozen stratification closure (12) (green) and imposing the effective stratification (13) from the simulation (red).

5. Conclusion

The problem of flame propagation in a tube filled with an axially stratified mixture has been investigated numerically and theoretically. The stratification cases considered are consistent with ignition scenarios above a liquid H_2 pool. It is shown that the mechanism responsible for flame acceleration in such scenarios remains essentially a wall confinement effect (finger-flame), similar to the homogeneous case, which can be either enhanced or mitigated depending on the gradient of reactivity imposed by the stratification. Two stratification parameters f_{ρ_b} and $f_{\sigma s_L}$ are shown to account for the impact of stratification on

the finger flame mechanism. The paper also highlights the large gap that can be observed between the effective stratification experienced by the flame and the stratification imposed before ignition, attributed to the piston effect induced by the flame on the unburnt mixture ahead of it. This gap is also larger with stronger initial stratification. This observation has strong implications for the problem of flame ignition in stratified mixtures, where the initial conditions are shown here to fail to properly characterize the impact on flame acceleration. Further work is needed to complement the theoretical derivation provided in this paper with a simple closure model for the effective parameters that would not hinder its practical use.

Novelty and significance statement

A combined numerical and theoretical investigation of the effect of axial mixture stratification –temperature and composition– on flame propagation in tubes is performed for the first time, in conditions consistent with the characteristics of reactive clouds above liquid-hydrogen pools. The work theoretically identifies two stratification parameters, directly linked to the strength and nature of the coupling (synergistic or competing) between stratification and wall confinement effects. The study also highlights that the impact of stratification cannot be properly characterized by the initial stratification conditions, with strong implications for the problem of flame ignition in stratified mixtures.

CRediT authorship contribution statement

Sébastien Missey: Numerical simulation, Formal analysis, Data analysis and processing, Writing – original draft. **Omar Dounia:** Conceptualization, Formal analysis, Writing – original draft, Supervision. **Laurent Selle:** Conceptualization, Formal analysis, Writing – review & editing, Supervision, Funding acquisition.

Declaration of competing interest

The authors declare that they have no known competing financial interests or personal relationships that could have appeared to influence the work reported in this paper.

Acknowledgments

This study has received funding from the PEPR-H_2 ESKHYMO. HPC resources from GENCI (Allocations A0132B10627)

Appendix A. Supplementary data

Supplementary material related to this article can be found online at https://doi.org/10.1016/j.proci.2024.105279.

References

[1] Interim Report on an Investigation of Hazards Associated with Liquid Hydrogen Storage and Use, Arthur D. Little, Inc, Cambridge, Massachusetts, 1959.
[2] R.D. Witcofski, J.E. Chirivella, Experimental and analytical analyses of the mechanisms governing the dispersion of flammable clouds formed by liquid hydrogen spills, Int. J. Hydrog. Energy 9 (5) (1984) 425–435.
[3] Preslhy, Prenormative research for safe use of liquid hydrogen, available at <https://preslhy.eu/>.
[4] A. Friedrich, A. Veser, G. Necker, J. Gerstner, N. Kotchourko, Pre-Normative Research for Safe Use of Liquid Hydrogen Pool-Experiments (WP3.4 and WP4.4), 2020.
[5] H. Cheikhravat, J. Goulier, A. Bentaib, N. Meynet, N. Chaumeix, C.E. Paillard, Effects of water sprays on flame propagation in hydrogen/air/steam mixtures, Proc. Combust. Inst. 35 (3) (2015) 2715–2722.
[6] L.R. Boeck, P. Katzy, J. Hasslberger, A. Kink, T. Sattelmayer, The GraVent DDT database, Shock Waves 26 (5) (2016) 683–685.
[7] M. Kuznetsov, A. Denkevits, A. Veser, A. Friedrich, Flame propagation regimes and critical conditions for flame acceleration and detonation transition for hydrogen-air mixtures at cryogenic temperatures, Int. J. Hydrog. Energy 47 (71) (2022) 30743–30756.
[8] X. Shen, W. Fu, W. Liang, J.X. Wen, H. Liu, C.K. Law, Strong flame acceleration and detonation limit of hydrogen-oxygen mixture at cryogenic temperature, Proc. Combust. Inst. 39 (2023) 2967–2977.
[9] L. Yang, Z. Chen, Effects of cryogenic temperature on premixed hydrogen/air flame propagation in a closed channel, Proc. Combust. Inst. 39 (2022) 2991–2999.
[10] T. Jordan, KIT, Pre-Normative Research for Safe Use of Liquid Hydrogen (PRESLHY) Experimental Investigation of Cryogenic Hydrogen Release and Mixing Deliverable Number: 3.3 (D20) Work Package: 3 Version: 1.0, 2021.
[11] I. Wierzba, K. Harris, G.A. Karim, Effect of low temperature on the rich flammability limits in air of hydrogen and some fuel mixtures containing hydrogen, Int. J. Hydrog. Energy 17 (2) (1992) 149–152.
[12] J.-J. Hok, O. Dounia, O. Vermorel, T. Jaravel, Effect of Flame Front Thermo-Diffusive Instability on Flame Acceleration in a Tube, 28th International Colloquium on the Dynamics of Explosions and Reactive Systems, 2022.
[13] V. Bychkov, V. Akkermana, G. Frua, A. Petchenko, L.-E. Eriksson, Flame acceleration in the early stages of burning in tubes, Combust. Flame 150 (4) (2007) 263–276.
[14] L.Y.M. Gicquel, N. Gourdain, J.F. Boussuge, H. Deniau, G. Staffelbach, P. Wolf, T. Poinsot, Calcul parallèle haute performance des écoulements en géométries complexes, C. R. - Mec. 339 (2011) 104–124.
[15] T.J. Poinsot, S.K. Lelef, Boundary conditions for direct simulations of compressible viscous flows, J. Comput. Phys. 101 (1) (1992) 104–129.
[16] Chemical-kinetic mechanisms for combustion applications, San Diego Mechanism web page, Mechanical and Aerospace Engineering (Combustion Research), University of California at San Diego, available at <http://combustion.ucsd.edu>.
[17] D.M. Valiev, V. Akkerman, M. Kuznetsov, L.E. Eriksson, C.K. Law, V. Bychkov, Influence of gas compression on flame acceleration in the early stage of burning in tubes, Combust. Flame 160 (1) (2013) 97–111, arXiv:1203.1396.
[18] S. Demir, H. Sezer, V. Akkerman, Effect of local variations of the laminar flame speed on the global finger-flame acceleration scenario, Combust. Theory Model. 22 (5) (2018) 898–912.